WORLD JOURNAL OF PHARMACEUTICAL RESEARCH
Coden USA: WJPRAP Impact Factor 8.63
Volume 15, Issue 13, 2143-2158. Research Article ISSN 2277–7105

SPEARMINT-MEDIATED GREEN SYNTHESIS OF TETRAGONAL MnO_2 NANOPARTICLES WITH ENHANCED ANTIMICROBIAL AND ANTIOXIDANT PROPERTIES

Khan Kadir Rafik[1], Pratiksha Shrichand Rathod[2], Neha Samreen Gulam Dastageer[2], Momin Nishat Parveen[1*]

[1,1*,2]Department of Chemistry, Sir Sayyed College of Arts, Commerce and Science, Chhatrapati Sambhajinagar (Aurangabad), 431001 M. H., India.

[2]Department of Chemistry, Milind College of Science, Chhatrapati Sambhajinagar (Aurangabad), 431001 M. H., India.

Article Received on 28 May 2026,
Article Revised on 25 June 2026,
Article Published on 01 July 2026

https://doi.org/10.5281/zenodo.23032296

***Corresponding Author**

Momin Nishat Parveen

Department of Chemistry, Sir Sayyed College of Arts, Commerce and Science, Chhatrapati Sambhajinagar (Aurangabad), 431001 M. H., India.

How to cite this Article: Khan Kadir Rafik[1], Pratiksha Shrichand Rathod[2], Neha Samreen Gulam Dastageer[2], Momin Nishat Parveen[1]*. (2026). Spearmint-Mediated Green Synthesis of Tetragonal MnO_2 Nanoparticles with Enhanced Antimicrobial and Antioxidant Properties. World Journal of Pharmaceutical Research, 15(13), 2143–2158.
This work is licensed under Creative Commons Attribution 4.0 International license.

ABSTRACT

Manganese dioxide nanoparticles (MnO_2 NPs) were successfully synthesized using a green approach with spearmint plant leaf extract. The synthesized nanoparticles were characterized using various spectroscopic techniques, including Fourier-transform infrared spectroscopy (FT-IR), ultraviolet-visible (UV-Vis) spectroscopy, scanning electron microscopy (SEM), high-resolution transmission electron microscopy (HRTEM), powder X-ray diffraction (XRD), and energy-dispersive X-ray (EDX) spectroscopy. XRD analysis revealed the tetragonal crystalline structure of the MnO_2 NPs with an average crystallite size of 24 nm. SEM images showed roughly spherical nanoparticles with diameters ranging from 25 to 146 nm, while HRTEM indicated an average particle size of 34 nm. FT-IR spectra confirmed the presence of Mn-O bonds, and EDX analysis verified the elemental composition of the nanoparticles. The biosynthesized MnO_2 NPs exhibited strong antimicrobial activity against various bacterial strains, including Staphylococcus aureus, Bacillus subtilis, Escherichia coli, and Klebsiella pneumoniae, with zones of inhibition ranging from 12 to 16 mm. However, the nanoparticles showed no antifungal activity against Aspergillus niger. In

addition, the MnO_2 nanoparticles showed high antioxidant activity, where Mn2 (95.20%) and Mn1 (95.06%) were more effective than ascorbic acid 1 (94.15%) and ascorbic acid 2 (92.14%) in DPPH radical scavenging activity. These findings suggest that green-synthesized MnO_2 NPs using spearmint plant leaf extract have potential applications as antimicrobial and antioxidant agents.

KEYWORDS: Green synthesis MnO_2 NPs, Antimicrobial and Antioxidant properties analysis.

1. INTRODUCTION

Nanomaterial's, defined as materials with a length scale of less than 100 nanometers, are becoming increasingly popular due to their fundamental scientific significance and the potential applications arising from their intriguing magnetic, electrical, and catalytic properties.[1-3] Manganese is the twelfth most abundant element in the earth's crust and is therefore relatively available, making it ideal for cost-effective large-scale applications. Manganese oxide nanoparticles can be prepared using both top-down and bottom-up approaches. However, the top-down approach is less commonly employed because of its high preparation costs and the structural defects it introduces in the manufactured nanoparticles.[4]

Most researchers favor the bottom-up method because particles with uniform sizes and morphologies can be collected using this method.[5-7] Manganese oxides, such as MnO, MnO_2, and Mn_3O_4, have been used in sensors, catalysis, rechargeable batteries, super-capacitors, and waste water treatment.[8,9] Owing to its high redox potential, high theoretical capacity, and low cost, MnO_2 has become a common cathode material in many types of batteries.[10] Therefore, employing biological methods, especially those derived from plants, for NP synthesis presents an alternative to traditional techniques.

Plants contain chemicals such as alkaloids, polyphenols, flavonoids, and terpenoids. These chemicals help convert metal ions into metal nanoparticles.[11-13] In this regard, the leaf extract of spearmint, a species of the mint family, was used for the bioconversion of manganese ions to NPs. Mint, in various forms, is used in medicine for its reputed digestive, antimicrobial, and anti-inflammatory properties. It is frequently used to relieve indigestion, irritable bowel syndrome (IBS), and other gastrointestinal issues.

Moreover, mint oil is a crucial component in products such as cough drops, inhalers, and even some tooth pastes and mouthwashes.[14,15] Using manganese sulfate as a precursor material, we present a precipitation technique for the manufacture of MnO_2 nanoparticles in the present study. The biological properties of the as-prepared MnO_2 NPs were investigated against various bacterial and fungal strains, including S. aureus, B. subtilis, E. coli, K. pneumonia and A. niger. The experimental procedure for the synthesis of MnO2 NPs using spearmint leaves extract is depicted in Figure 1.

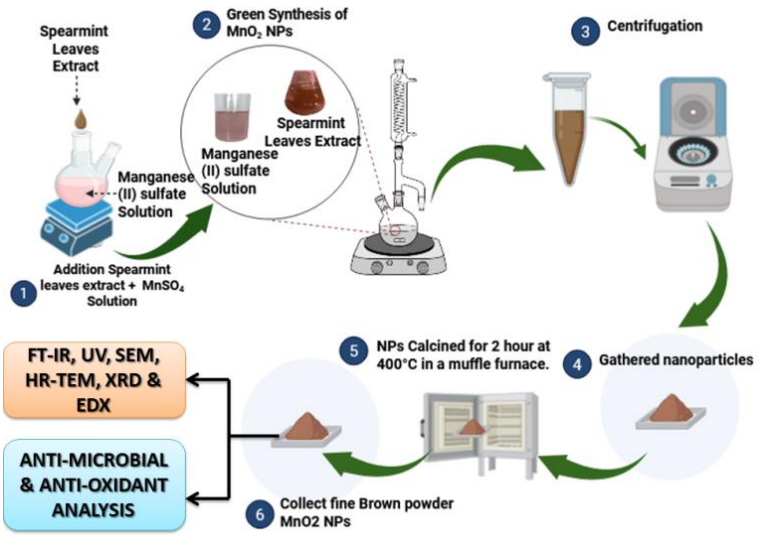

Figure: 1. Schematic Representation for Spearmint Plant Leaves Mediated Green Synthesis of MnO_2 NPs.

2. MATERIALS AND METHODS

Manganese (II) sulfate monohydrate (99% purity) were purchased from Sigma-Aldrich, Merck and Molychem companies of high purity and used directly in the reaction protocol without further purification.

2.1. Collection of the Plant Material

Spearmint was acquired from the Shahaganj Chh.Sambhajinagar (Aurangabad) local market, and the spearmint leaves were cut and washed with tap water and distilled water to remove the dust particles and other possible contaminants, and then dried at room temperature. They were finally crushed in a mixer grinder, and the powder was passed through a Strainer Sieve.

Preparation of Leaves Extract

The plant extract was made using the previously described procedure, with a few minor adjustments.[16] The plant was extracted by combining 10 g of dried spearmint leaves with 100 ml of double-distilled water in a 250 ml beaker. The container was placed on an electric magnetic stirrer at 80-90°C and 300 rpm for 1 h. After cooling to room temperature, the solution was filtered through Whatman No.1 filter paper.

2.3. Green synthesis of MnO_2 Nanoparticles

Metallic NPs were prepared using a previously reported protocol.[17], with a few modifications. In short, 10 mL of the precursor manganese (II) sulfate and 90 mL of the spearmint leaves extract were combined at 80°C while being constantly stirred. The extract was transparent before the addition of the salt solution. The extract turned murky when the salt solution was added. The solution turned dark brown over time, indicating the formation of metallic nanoparticles. A UV-Visible and FT-IR spectrophotometer was used to confirm the findings. The nanoparticles were recovered by centrifugation at 6500 rpm for 15 minutes after a 24-hour period. To remove soluble contaminants, the gathered nanoparticles were rinsed twice using distilled water and ethanol. This precipitate was subsequently calcined for 2 hour at 400°C in a muffle furnace, resulting in a fine brownish powder, which was carefully preserved for future research.

2.4. Characterization

Fourier transform infrared (FTIR) spectroscopy (Thermo Nicolat 6700, U.S.) was used to characterize the manufactured materials. The examination was conducted within the wavenumber range of 4000 cm−1 to 500 cm−1. The absorption spectra at the 800–200 nm scanning range were obtained using the UV-Visible absorption spectrophotometer (JASCO UV V-750). The characteristic absorption spectra demonstrate the continual production of MnO_2-NPs. X-ray diffraction (Brukar D8-Advanced Diffractometer) was used to crystallographically clarify MnO_2 NPs, and FE-SEM (Nova Nano-SEM NPEP303) and TEM (PHILIPS CM200) were used to analyze morphological features, such as size and topology. The chemical purity and elemental composition were determined by energy dispersive X-ray spectroscopy (EDX, Bruker, XFlash 6I30), Using a disk diffusion experiment, the antibacterial activity of the biosynthesized MnO NPs was evaluated against two Gram-positive bacteria, Staphylococcus aureus and Bacillus subtilis and two Gram-negative bacteria, Escherichia coli and Klebsiella pneumonia bacteria. The findings were compared

using Streptomycin (10 micrograms per disk) as the reference standard. The antibacterial activity was tested using nutritional agar from Hi- media. Composition (gL-1). Sodium chloride 5.0: Beef extract 10.0: Penton 10.0 (pH 7.2). The diameter of the Zone is measured by Vernier Calliper.

The antioxidant activity of the synthesized nanoparticles was evaluated using the DPPH free radical scavenging assay. The nanoparticles exhibited significant radical scavenging activity in a concentration-dependent manner. The percentage inhibition increased with increasing concentration, indicating strong antioxidant potential. The IC_{50} value was found to be lower compared to the standard antioxidant (ascorbic acid), suggesting effective free radical neutralization ability.

3. RESULTS AND DISCUSSIONS

3.1. Visible Observation

The extract is normally yellowish-green prior to reaction due to the presence of chlorophyll, flavonoids, and polyphenols. After reaction with manganese (II) sulfate solution, the color changes from yellowish-green to dark brown. This color change confirms the reduction of manganese ions and the formation of manganese oxide, or Mn NPs.[18]

3.2. Fourier transform infrared spectroscopy of Spearmint Plant Leaves Extract and MnO_2 NPs

The primary peak in the spectrum was found at 3275 cm^{-1}, with other peaks at 2950, 2390, 1635, 1350, 1150, and 970 cm^{-1}, respectively. The spectral ranges and associated band assignments of the extracts from spearmint leaves are listed in Table 1. Spearmint leaves contain hydrogen-bonded alcohol, phenols, alkanes, alkenes, alcohol, ethers, and carbonyl groups. Hydrogen-bonded alcohols and phenols are found in the bands at 3275 cm^{-1}. The presence of the 2950 cm^{-1} C-H stretch in spearmint leaves confirms the presence of these saturated carbon-containing compounds within the plant material[19]. The band at 2390 cm^{-1} indicates the presence of nitrile groups (C≡N stretching). The vibrational absorption band at 1635 cm^{-1} was assigned to the C=O stretching. A notable band at 1350 cm^{-1} and 1150 cm^{-1} can be assigned to C-H bending, C-O & C-N bending respectively, A band at 970 cm^{-1} represent the (–HC=CH–trans-) bending vibrations, These groups are commonly found in various terpenoids, including those present in Spearmint leaves.[20-23]

Table: 1. FTIR Spectrum Analysis of Spearmint Plant Leaves Extract.

Wave numbers (cm-1)	Assignments
3275 cm^{-1}	-OH stretch
2950 cm^{-1}	C-H stretch
2390 cm^{-1}	C≡N stretch
1635 cm^{-1}	C=O stretch
1350 cm^{-1}	C-H bending
1150 cm^{-1}	C-O & C-N bending
970 cm^{-1}	(–HC=CH– trans-) bending vibrations

MnO_2 NPs show Broad peaks are obtained at 2350, 1132, 829,594 and 427; these peaks are related to the presence of O-H, C=O, C-C, Mn-C, Mn-O bonds on the surface of manganese dioxide nanoparticles.[24-26] The peak at 427 cm^{-1} in the MnO_2 nanoparticle FT-IR spectra is attributed to Mn–O stretching or bending vibrations, reflecting the MnO_2 structure and confirming its successful synthesis. Figure 2 displays the FT-IR spectrum of spearmint plant leaves and MnO_2 NPs, covering the wavenumber range of 400-4000 cm^{-1}.

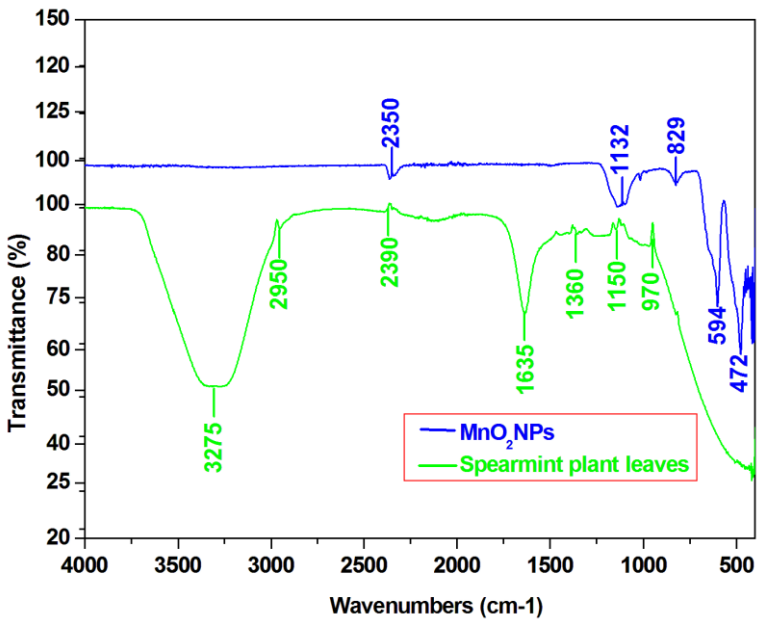

Figure: 2. FT-IR spectrum of Spearmint Plant Leaves & MnO_2 NPs.

3.3. UV-Visible spectroscopy of MnO_2 NPs

The UV–vis spectra of MnO2 nanoparticles are shown in Fig. 3. It showed absorption peaks at 243 and 255 nm. These are in the UV region and are typically associated with charge transfer transitions, most likely $O^{2-} \rightarrow Mn^{4+}$ ligand-to-metal charge transfer (LMCT) in MnO_2 or other manganese oxides. In nanoparticles, these peaks can appear slightly shifted compared to bulk MnO_2 due to quantum size effects and surface states of the nanoparticles

and 340 nm, which is in the Near-UV region and is often attributed to d–d electronic transitions within Mn ions (like Mn^{4+} or Mn^{3+}) in an octahedral oxide environment, or to defect/surface plasmon-like resonance if the particle size is very small and surface defects are significant. For manganese oxides, this peak can also arise from intervalence charge transfer ($Mn^{3+} \leftrightarrow Mn^{4+}$) between different oxidation states in the lattice. Peaks in these regions represent π-π*, n-π*, or d-d electronic transitions.[27-29]

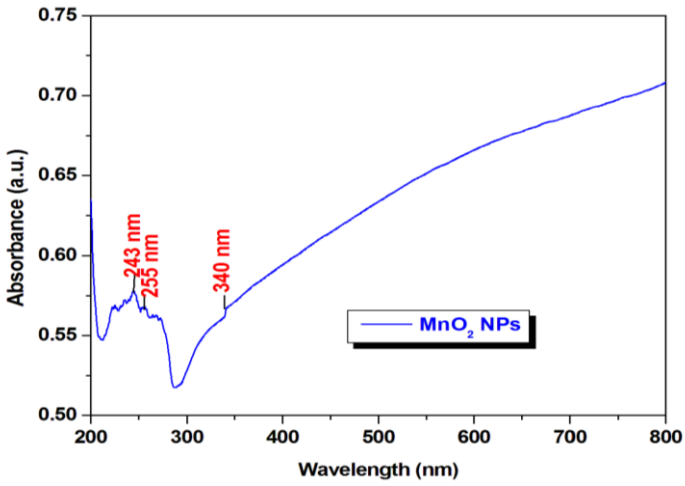

Figure: 3. UV-visible spectrum of MnO_2 NPs.

3.4. Powder X-Ray diffraction (XRD)

X-ray diffraction spectroscopy was used to analyze the crystalline structure of the prepared MnO_2 NPs, as shown in Figure 4. The diffraction peaks at 2θ of prepared nanoparticles were 18.34°, 25.74°, 28.78°, 37.66°, 42.14°,45.50°, 48.80°, 56.44°, 65.26°, and 69.64° which correspond to crystal planes of (110), (200), (310), (211), (301), (411), (600), (521), (541) and (222) respectively. This suggests that the tetragonal crystalline structure of the MnO_2 nanoparticles was successfully prepared, which agrees well with the JCPDS card number (44-0141).[30]

Using the Debye–Scherrer equation, the average crystallite size of the particles was determined to be 24 nm.[31]

Debye–Scherrer equation: $D = K\lambda / (\beta \cos \theta)$

Where β is the full-width half maximum, k is the Scherrer constant, D is the crystallite size, and λ is the wavelength of the X-ray.

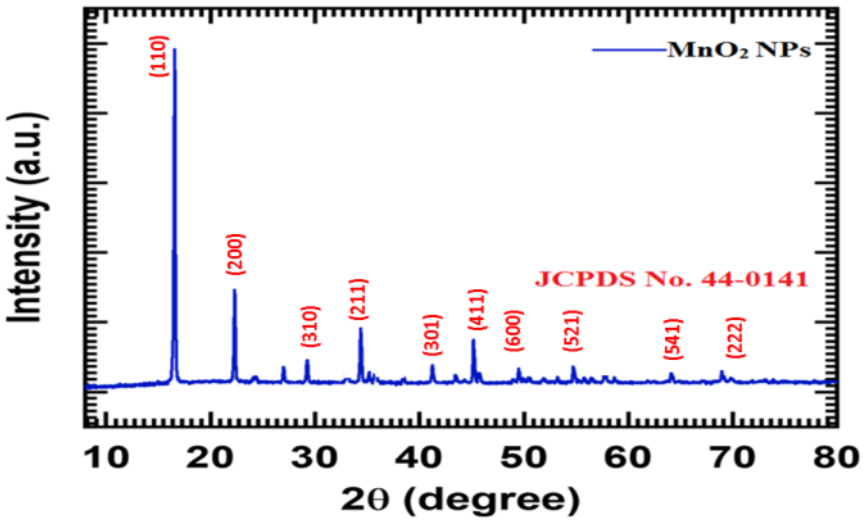

Figure: 4. XRD spectrum of MnO_2 NPs.

3.5. Energy Dispersive X-Ray (EDX) and Mapping Images

Energy-dispersive X-ray (EDX) spectral analysis of the synthesized MnO_2 nanoparticles confirmed the presence of manganese (Mn), oxygen (O), carbon (C), and nitrogen (N) (Fig. 5b). The results of EDX elemental image mapping shown in (Fig. 5a) revealed the atomic percentages of Mn, O, C, and N in the synthesized MnO_2 nanoparticles. It shows a peak for Mn-O linkage at 0.2688 keV. The production of Mn dioxide NPs is confirmed by the elemental peaks of manganese and oxygen. These EDX features are consistent with previous studies.[32-34]

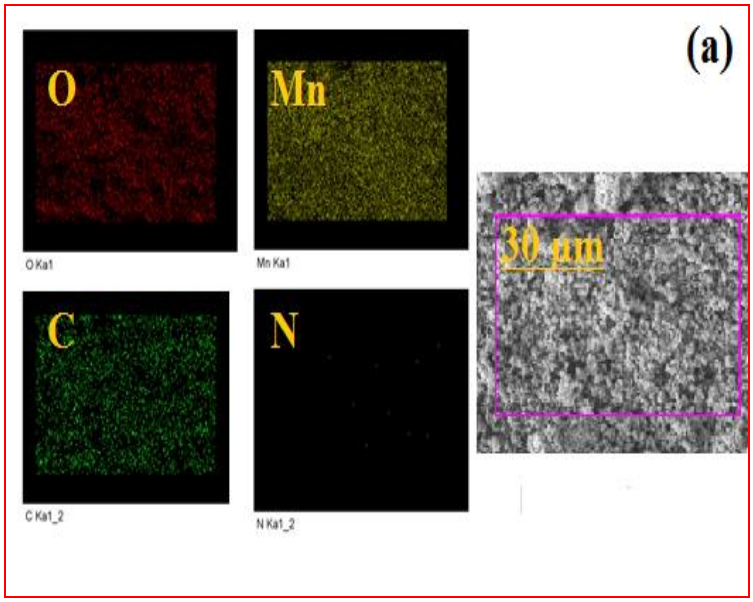

Figure: 5. (a) Elemental mapping images of MnO_2 Nps.

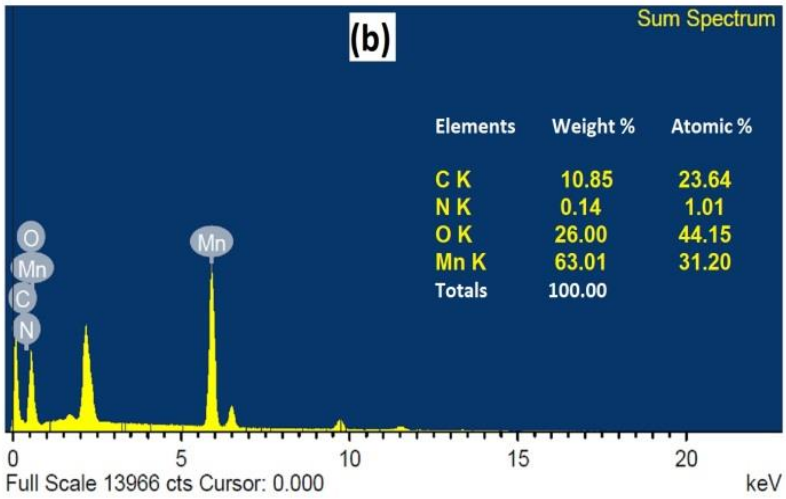

Figure: 5. (b) EDX and Percentages of Mn, O, C, and N.

3.6. Field Emission Scanning Electron Microscopy (FE-SEM)

The produced MnO_2 NPs' surface morphological and size characteristics were examined using a scanning electron microscope (SEM). The FE-SEM images of an MnO_2 nanoparticle are shown in Figure (6). The synthetic sample almost roughly spherical form and nanoscale dispersion are seen in the image.[35-37] The diameters of the nanoparticles observed were 25 to 146 nm, as shown in figure 6. These pictures confirm the formation of MnO_2 nanoparticles.

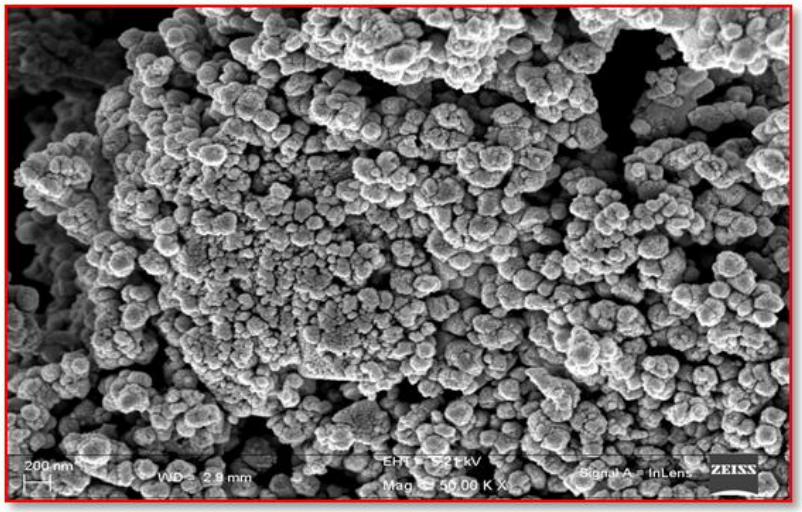

Figure: 6 FE-SEM images of a MnO_2 NPs.

3.2.6. High-resolution Transmission Electron Microscopy and Selective area Electron Diffraction (HRTEM-SAED)

Figure (7a) shows a TEM photograph of the prepared sample. The product was found to include particles of diverse sizes and shapes, indicating that aggregates had developed. MnO_2

nanoparticles have an average size of around 34.94 nm. HR-TEM images (Figures 7b and 7c) show clear lattice fringes with an estimated d-spacing of 0.280 nm, confirming the tetragonal crystalline structure. The diffraction ring point in the SAED pattern suggests phase selection based on the materials' crystallinity (Figure 7d).[38, 39] Thus, the XRD results were equivalent. The images were created by research of TEM features, followed by material analysis using ImageJ software.

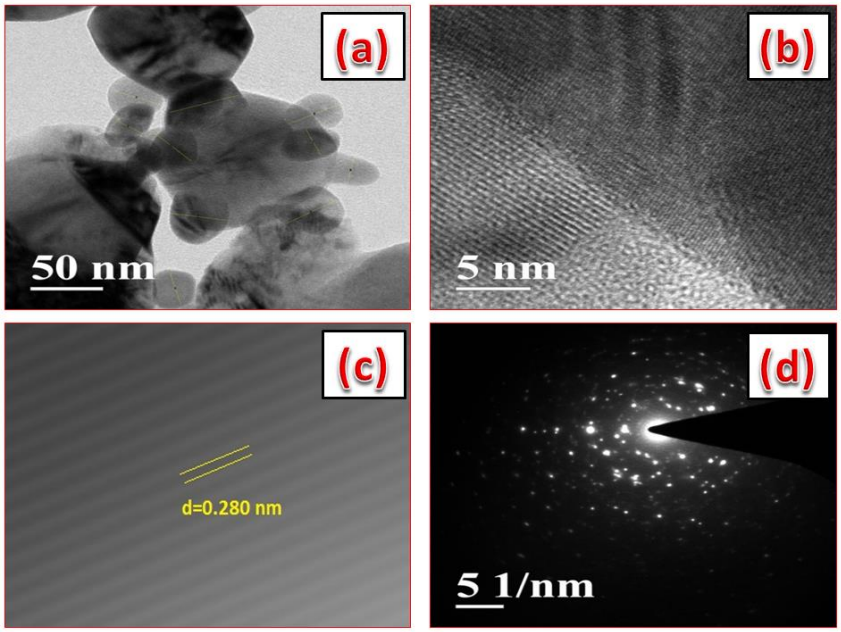

Figure: 7. (a) TEM, (b) HRTEM, (c) d-spacing calculations of the prepared MnO_2 NPs and (d) SAED.

3.7. Antimicrobial Activity

Research has explored the antibacterial properties of the biosynthesized MnO_2 nanoparticles against Aspergillus niger, Bacillus subtilis, Escherichia coli, Klebsiella pneumoniae, and Staphylococcus aureus. The antimicrobial effectiveness of these nanoparticles was evaluated by measuring the diameter of the inhibition zone using the disc diffusion method. Inhibition zones were observed for all tested microorganisms, indicating that manganese oxide nanoparticles can potentially serve as antimicrobial agents. Figure 8 shows the impact of manganese oxide nanoparticles on the growth of bacterial and fungal strains, while Table 2 shows the inhibition zone values.

The antibacterial activity analysis revealed a 14 mm zone of inhibition for Gram-positive S. aureus and a 16 mm zone for B. subtilis. Similarly, Gram-negative E. coli and K. pneumoniae exhibited zones of inhibition measuring 12 and 13 mm, respectively. However, the antifungal

activity analysis of A. niger did not show any zone of inhibition. For long-term performance, the activity is also dependent on the NPs' physicochemical characteristics. In general, the particle dosage, length of therapy, and method of delivery affect the effectiveness of antibacterial activity.[40, 41]

Table: 2. Antimicrobial activity of Synthesized MnO_2 Nanoparticles against Pathogenic Bacterial and Fungal Species.

Microbes	Strain reference	Zone Of Inhibition (mm)	
		Concentration 1mg/ml	
		Streptomycin [+ve control]	MnO_2 NPs
S. aureus	NCIM 2079	23	14
B. subtilis	NCIM 2250	32	16
E. coli	ATCC 25922	23	12
K. pneumoniae	NCIM 2719	28	13
A. niger	ATCC 16404	16	-

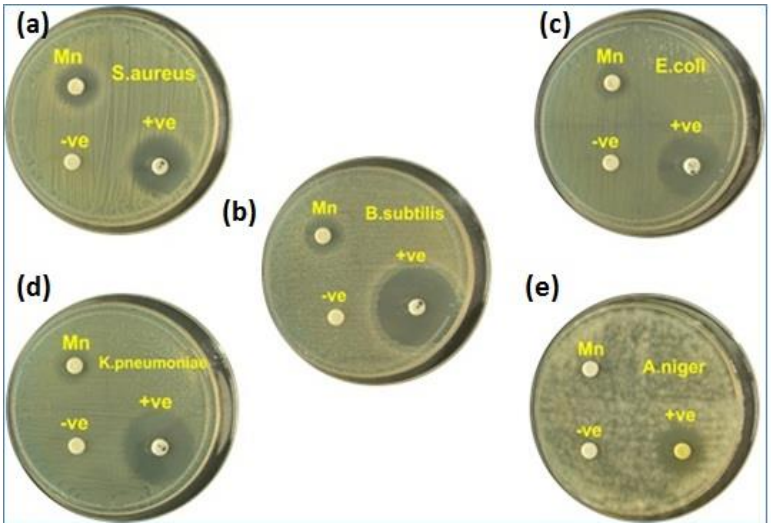

Figure: 8. Antimicrobial effect of biologically synthesized MnO_2 NPs against (a) S. aureus, (b) B. subtilis, (c) E. coli, (d) K. pneumoniae, (e) A. niger.

3.8. Antioxidant activity

The antioxidant potential of the biosynthesized MnO_2 nanoparticles (MnO_2 NPs) was evaluated using the DPPH radical scavenging assay.[42-45] The DPPH (2,2-diphenyl-1-picrylhydrazyl) method is a simple and widely accepted technique for assessing antioxidant activity. The results demonstrated that both Mn-based nanoparticles exhibited significant

antioxidant activity, with Mn1 showing high inhibition (95.06%), followed by Mn2 (95.20%), which were comparable to the standard ascorbic acid (94.15%) (Table 3). These findings indicate that the synthesized MnO_2 nanoparticles possess strong free radical scavenging ability and can act as effective antioxidant agents.

Table: 3. Scavenging Effect on DPPH Radical and % Inhibition of Synthesized MnO_2 NPs.

Compound Code	3.9	7.8	15.6	31.3	62.5	125	250	500	Mean
Mn1	90.90	91.95	94.60	94.99	95.98	96.39	97.40	98.30	**95.06**
Mn2	91.58	92.90	93.78	94.99	95.60	96.78	97.79	98.20	**95.20**
Ascorbic acid 1	91.58	92.18	93.59	94.19	95.39	96.70	97.40	98.20	**94.15**
Ascorbic acid 2	86.70	87.78	88.60	91.94	93.73	95.02	96.02	97.30	**92.14**

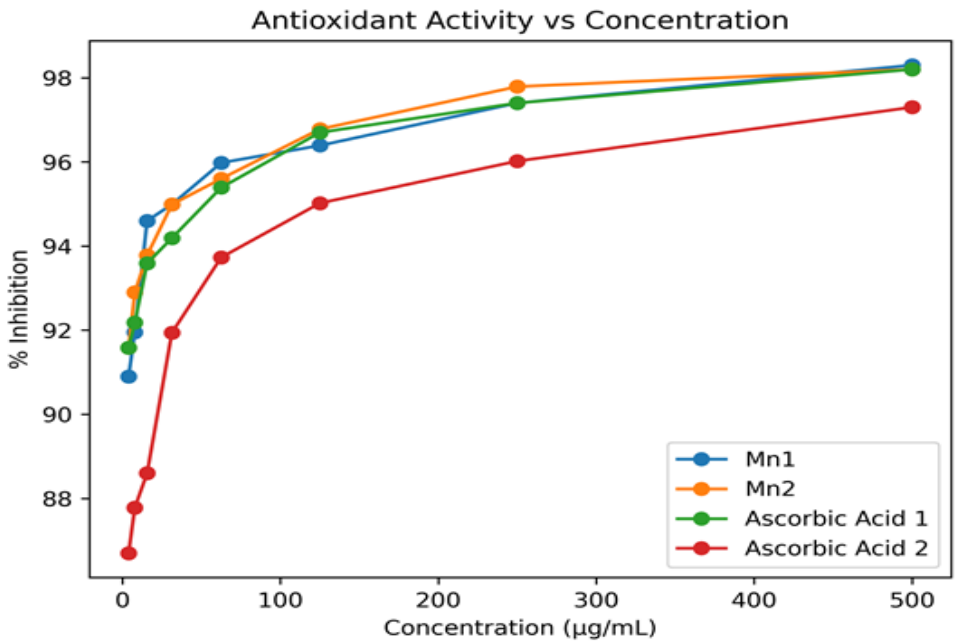

Figure: 9. DPPH Scavenging Activity of MnO_2 Nanoparticles and Ascorbic Acid.

4. CONCLUSIONS

Manganese dioxide nanoparticles (MnO_2 NPs) were successfully synthesized using a green method with spearmint leaf extract. XRD analysis revealed an average crystallite size of ~24 nm. SEM images showed a roughly spherical morphology with particle sizes ranging from 25 to 146 nm, while HRTEM analysis indicated an average size of ~34 nm. The SAED pattern confirmed the crystalline nature of the nanoparticles.

FT-IR spectra exhibited a characteristic Mn–O absorption band at 427 cm^{-1}, confirming nanoparticle formation. EDX analysis further revealed the presence of Mn, C, N, and O elements.

The synthesized MnO_2 nanoparticles demonstrated effective antibacterial activity against Klebsiella pneumoniae, Bacillus subtilis, Escherichia coli, and Staphylococcus aureus. Additionally, they showed significant antioxidant activity, indicating strong free radical scavenging potential.

Overall, this study confirms that green-synthesized MnO_2 nanoparticles possess promising antibacterial and antioxidant properties, making them suitable for potential biomedical and environmental applications.

ACKNOWLEDGMENTS

The authors respectfully thank the Principal and the Head of the Department of Chemistry for continuously providing the necessary research facilities. The authors are also grateful to the professors and all faculty members of the Department of Chemistry at Milind College of Science, Nagsenvana, Chh. Sambhajinagar (Aurangabad), India, for their guidance and support during this research work.

REFERENCES

1. Shagufta Ali, Muhammad Imran, Rehana Kousar, Mahvish Fatima, Muhammad Zeewaqar Manzoor, Hafiz Ejaz Ahmed, Shehla Riaz, Hafeez Ullah, Aalia Nazir, Zahida Batool, Desalination Water Treat. 2024; 320: 100688 https://doi.org/10.1016/j.dwt.2024.100688.
2. D. Astruc, Chem. Rev., 2020; 120: 461. https://doi.org/10.1021/acs.chemrev.8b00696
3. S. Jadoun, R. Arif, N. K. Jangid, and R. K. Meena, Environ. Chem. Lett., 2021; 19: 355. https://doi.org/10.1007/s10311-020-01074-x.
4. I. Khan, K. Saeed, and I. Khan, Arab. J. Chem., 2019; 12: 908 https://doi.org/10.1016/j.arabjc.2017.05.011.
5. V. Yadav et al., Curr. Nanomater., 2025; 10: 78 https://doi.org/10.2174/2405461508666230627144618.
6. R. M. de Boer, M. A. van Huis, and R. G. Mendes, Small, 2024, 20 https://doi.org/10.1002/smll.202304925.

7. W. M. Saod et al., Biotechnol. Rep., 2022; 34: e00729. https://doi.org/10.1016/j.btre.2022.e00729.
8. Y. Guo, Y. Zhang, and H. Lu, Battery Energy, 2022; 1. https://doi.org/10.1002/bte2.20210014.
9. D. Ociński, I. Jacukowicz-Sobala, P. Mazur, J. Raczyk, E. Kociołek-Balawejder, Chem. Eng. J., 2016; 294: 210. https://doi.org/10.1016/j.cej.2016.02.111.
10. Xilin Xiao, Lei Zhang, Wenli Xin, Min Yang, Yaheng Geng, Mengfan Niu, Hui Zhang, Zhiqiang Zhu, Small, 2024; 20. https://doi.org/10.1002/smll.202309271.
11. H. Y. Zhang, D. X. Cao, and X. Bai, J. Power Sources, 2019; 444: 227299.
12. B. W. Byles and E. Pomerantseva, Proc. SPIE, 2016; 9924: 992406.
13. 13. A. Ciorîță, M. Suciu, S. Macavei, I. Kacso, I. Lung, M. L. Soran, Molecules, 2020; 25: 819. https://doi.org/10.3390/molecules2504081914.
14. S. A. Khan, S. Shahid, B. Shahid, U. Fatima, S. A. Abbasi, Biomolecules, 2020; 10: 785. https://doi.org/10.3390/biom10050785.
15. S. Gharehyakheh A. Ahmeda, A. Haddadi, M. Jamshidi, M. Nowrozi, M. M. Zangeneh,, Appl. Organomet. Chem., 2020; 34: e5492. https://doi.org/10.1002/aoc.5492.
16. L. Zhang Y. Chen, Z. J. Li, X. Li, G. Fan,, Food Funct., 2022; 13: 3110. https://doi.org/10.1039/D1FO04080D.
17. M. H. Milani A. Mohammadi, S. Panahirad, H. Farhadi, P. Labib, M. Kulak, G. Gohari, V. Fotopoulos, F. Vita,, Plants, 2024; 13. https://doi.org/10.3390/plants13202934.
18. J. Singh A. Mehta, M. Rawat., J. Environ. Chem. Eng., 2018; 6: 1468. https://doi.org/10.1016/j.jece.2018.01.054.
19. S. A. Prasad, Mater. Sci. Semicond. Process., 2017; 71: 342. https://doi.org/10.1016/j.mssp.2017.08.020.
20. B. L. Koop M. Nascimento da Silva, F. Diniz da Silva, K. T. S. Lima, L. S. Soares, C. J. Andrade, G. A. Valencia, A. R. Monteiro,., Food Res. Int., 2022; 153. https://doi.org/10.1016/j.foodres.2021.110929.
21. N. C. Joshi ,V. Rangar, R. Sati, E. Joshi, A. Singh,, Orient J. Chem., 2019; 35: 591.
22. S. Das, A. Das, R. T. Selvan, S. A. Raj, B. J, J. Textile Inst., 2021; 112: 1181. https://doi.org/10.1080/00405000.2020.1805194.
23. C. Savitha, T. Vigneshwari, C. R. Priyanka, S. Keerthika, A. S. Stanley, Acta Sci. Pharm. Sci., 2019; 3: 153. https://doi.org/10.31080/asps.2019.03.0290.
24. O. Taylan, N. Cebi, and O. Sagdic, Foods 2021; 10. https://doi.org/10.3390/foods10020202 P.

25. P. K. Jain, A. Soni, P. Jain, J. Bhawsar, J. Chem. Pharm. Res., 2016; 8: 1.
26. Y. T. Amara, M. Beldjilali, F. Z. Kermezli, I. Chikhi, I. Taha, I. Ismail, L. Belarbi, S. Bousalem, New J. Chem., 2023; 47: 13841. https://doi.org/10.1039/D3NJ01737K.
27. Y. Sun, Y. Wang, Y. Liu, H. Wang, C. Yang, X. Liu, F. Wang, Adv. NanoBiomed Res., 2023; 3. https://doi.org/10.1002/anbr.202200093.
28. R. M. de Boer, M. A. van Huis, and R. G. Mendes, Small, 2024; 20. https://doi.org/10.1002/smll.202304925.
29. H. Fouad, L. Hongjie, D. Hosni, J. Wei, G. Abbas, H. Ga'al, J. Jianchu, Artif. Cells Nanomed. Biotechnol. 2018; 46: 558. https://doi.org/10.1080/21691401.2017.1329739.
30. S. Chatterjee, A. Ja, A. Subramanian, S. Subramanian, J. Ind. Pollut. Control, 2017; 33: 1627.
31. J. R. Rajabathar, H. A. Al-Lohedan, P. Arunachalam, Z. A. Issa, M. K. Gnanamani, J. N. Appaturi, S. N. Ibrahim, W. M. Dahan, J. Alloy. Compd., 2020; 850: 156346. https://doi.org/10.1016/j.jallcom.2020.156346.
32. E. Ouda, N. Yousf, H. S. Magar, R. Y. A. Hassan, E. S. M. Duraia, J. Mater. Sci. Mater. Electron. 2023; 34.
33. Q. He, J. Liu, X. Liu, G. Li, D. Chen, P. Deng, J. Liang, Electrochim. Acta 2019; 296: 683. https://doi.org/10.1016/j.electacta.2018.11.096.
34. A. O. Bokuniaeva and A. S. Vorokh, J. Phys.: Conf. Ser., 2019; 1410: 012057. https://doi.org/10.1088/1742-6596/1410/1/012057.
35. A. Ekinci, S. Kutluay, O. Şahin, O. Baytar, Int. J. Phytoremediation 2023; 25: 789. https://doi.org/10.1080/15226514.2022.2109588.
36. E. C. Devi and I. Soibam, Adv. Mater. Proc., 2021; 2: 93. https://doi.org/10.5185/amp.2017/206.
37. G. Sharma, A. Kumar, M. Naushad, Carbohydr. Polym., 2018; 202: 444. https://doi.org/10.1016/j.carbpol.2018.09.004.
38. E. Karu, B. Magaji, R. Atiko, F. Bala,Dutse J. Pure Appl. Sci., 2024; 10: 161. https://doi.org/10.4314/dujopas.v10i2a.15.
39. B. Magaji, R. Atiko, F. Bala., J. Appl. Pharm. Sci., 2015; 5: 105. https://doi.org/10.7324/JAPS.2015.501218.
40. P. P. J. Paul, M. Sakunthala, I. C. Udhaya, Int. J. Bot. Stud., 2017; 5: 71.
41. M. A. Veena, C. M. Hemanth Kumar, S. S. Majani, N. N. Munirajappa, B. Harendra, C. Shivamallu, H. L. Raghavendra, A. A. Shati, M. Y. Alfaifi, S. E. I. Elbehairi, Namratha, S. Prasad Kollur, Results Chem., 2024; 7. https://doi.org/10.1016/j.rechem.2023.101290.

42. D. Zhang, J. Dai, J. Zhang, Y. Zhang, H. Liu, Y. Xu, J. Wu, P. Li, ACS Omega 2024; 9: 18032. https://doi.org/10.1021/acsomega.3c09725.
43. EUCAST, Disk Diffusion Methodology v12.0, (2020), www.eucast.org.
44. CLSI, Performance Standards for Antimicrobial Susceptibility Testing, 33rd ed., (2023)
45. H. H. Farhan and A. M. Mohammed, Results Chem., 2024; 7. https://doi.org/10.1016/j.rechem.2023.101266.